Permeation Properties of Poly(*m*-xylene adipamide) Membranes

Camille Lixon Buquet,*,†,‡ Bessem Ben Doudou,‡ Corinne Chappey,† Eric Dargent,‡ and Stéphane Marais†

Laboratoire PBS, FRE 3101 CNRS, MPBM, FR 3038, Université de Rouen, Boulevard Maurice de Broglie, 76821 Mont Saint Aignan Cedex, and Laboratoire PBS, FRE 3101 CNRS, LECAP, Institute for Materials Research, Université de Rouen, Avenue de l'Université BP 12, 76801 Saint Etienne du Rouvray

Received: November 21, 2008; Revised Manuscript Received: January 22, 2009

The permeation properties of a semiaromatic polyamide, the poly(*m*-xylene adipamide) (MXD6), were investigated by water and carbon dioxide permeation experiments (pervaporation and gas permeation tests). Complementary microstructure informations were obtained from calorimetric measurements. Amorphous and semicrystalline MXD6 membranes were studied. The analysis of the water flux through amorphous MXD6 membranes showed a plasticization phenomenon followed by a water-induced crystallization. It resulted that the role played by water in these materials was complex because of the dependence of the water diffusivity on water concentration and time. Because of the presence of crystalline phase, a significant reduction of water and gas permeability of MXD6 and an increase in the delay of diffusion were observed. In terms of barrier properties for water and carbon dioxyde, MXD6 membrane crystallized at high temperature were more performant than water-induced crystallized ones. Correlations between microstructure and transport properties had been so established.

Introduction

For packaging materials, high barrier polymers are usually recommended. In particular for low-carbonated drinks, it is necessary to increase the barrier effect of the poly(ethylene terephthalate) (PET) to the oxygen and the carbon dioxide molecules. The gas barrier properties of PET are improved either by surface treatment such as acetylene plasma,[1] oxide treatments like silicon oxide,[2] and alumina oxide,[3] by including nanoclays[4] or by blending with gas barrier polymers.[5]

In the last decade, a new semiaromatic polyamide, poly(*m*-xylene adipamide) MXD6 has been developed.[6,7] Because of the high gas barrier properties, MXD6 was used with PET in multilayer form for blow molded bottles[8] or by mixing. As PET, MXD6 had a low crystallinity rate.[9] So, depending of the material thermal history, a wholly amorphous or a semicrystalline MXD6 could be obtained[10] at room temperature. Polyamides however absorbed water because of the amide functionality.[11] The water sorption resulted in a dimensional change and the reduction of the glass transition temperature (T_g).[12,13] When T_g decreased below room temperature, the polyamides showed lower stiffness, higher toughness, and lower electrical resistivity[14] since the amorphous phase had been softened by the plasticizing effect due to the absorbed water molecules. The role played by water in the amorphous state of MXD6 was therefore important and led to diffusion mechanisms which evolved during the water permeation process. We had shown in a previous work[15] that when T_g raised the room temperature, a crystalline phase appeared in the initially amorphous material. This water-induced crystallization did not differ from the classical thermal crystallization in term of crystallographic parameters. In the two cases, a spherolitic semicrystalline structure was obtained but the crystalline phase perfection was higher for the crystallization at high temperature than for the water-induced crystallization (at room temperature). The permeation behavior was then characterized by a dependence of the diffusivity with water concentration (plasticization) and with time (crystallization). In terms of application, such as fizzy drinks, the enhancement of barrier properties of polymer bottles was recommended. In that way, it was necessary to study the water and gas permeation properties as a function of the structural state of the MXD6 membrane.[16]

In this paper, the transport properties of MXD6 membranes were investigated by water and carbon dioxide permeation measurements: pervaporation and gas permeation tests while microstructural informations were obtained from calorimetric measurements. By this way, correlations between structure and transport properties were established. For that, various MXD6 membranes were analyzed in permeation: amorphous membrane, water-induced crystallized membrane and thermally crystallized membrane. Moreover two types of diffusing molecules were used, carbon dioxide and water. Indeed, water molecules were able to plasticize a polymer matrix such as a polyamide material[17] while carbon dioxide molecules were well known to not interact with it.

Experimental Methods

1. Material. Poly(*m*-xylene adipamide) or MXD6 (Figure 1) used in this study was supplied by Mitsubishi Gas Chemical Co (MXD6 6007) with a number-average-molecular weight of 25 000 mol·g^{-1}. The glass transition and melting temperature of the dry material were T_g = 82 °C and T_f = 238 °C, respectively. It was produced through polycondensation of meta-xylene Diamin with adipic acid. It was the only aliphatic polyamide resin which contained meta-xylene groups in the molecule as shown in Figure 1. Before experiments, the MXD6 pellets were dried at 80 °C for 24 h in a vacuum oven. The

* To whom correspondence should be addressed. E-mail camille.lixon@etu.univ-rouen.fr.

† Laboratoire PBS, FRE 3101 CNRS, MPBM, FR 3038, Université de Rouen.

‡ Laboratoire PBS, FRE 3101 CNRS, LECAP, Institute for Materials Research, Université de Rouen.

10.1021/jp810241z CCC: $40.75
Published on Web 02/23/2009

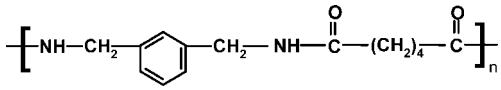

Figure 1. Repeating unit of MXD6.

membranes were obtained with the help of a compression molding apparatus with aluminum sheets heated at 280 °C. The pellets were compressed at 150 bar during 5 min followed by a quench to 0 °C in ice water. This procedure permitted to obtain wholly amorphous samples (it had been controlled by X-ray and differential scanning calorimetry analysis). Thermally crystallized MXD6 membranes were obtained after an annealing during 3 h for temperatures T_c included between T_g and T_f. Crystallization occurred and the degree of crystallinity was determined by a classical DSC procedure. By this way, the obtained degrees of crystallinity were included between 22 and 30%.

2. Methods

2.1. DSC Measurements. The thermal behavior of samples was investigated by using the conventional differential scanning calorimeter TA Instrument Q100. Samples with a mass of 10 ± 1 mg were used. The heating and cooling rates were 10 and 200 °C·min^{-1}, respectively. All DSC runs were carried out under nitrogen atmosphere to minimize the oxidative degradation. Before all DSC experiments, the baseline was calibrated using empty aluminum pans, and the DSC apparatus was calibrated using melting temperature and enthalpy of a high-purity indium standard (156.6 °C and 28.45 J·g^{-1}). From DSC analysis, it was possible to determine the characteristic temperature of the thermal event as glass transition, cold crystallization, and fusion. A study of the crystallization and the melting behavior of similar MXD6 samples were presented elsewhere.[10] From melting and crystallization enthalpies, it was possible to determine the degree of crystallinity X_c of the various samples.

2.2. Permeation Measurements. ***a. Water Permeation.*** The transport of water through MXD6 was studied by permeation tests (liquid water at $T = 25$ °C) with amorphous membranes of different thickness ($L = 76$, 114, and 128 μm) and with a thermally crystallized membrane ($L = 101$ μm). The water specific-permeameter consisted of a measurement cell, a dry nitrogen supply, and a chilled mirror hygrometer (General Eastern Instruments, MA) used for its high accuracy (0.07 ppm (volume) of water vapor in a gas). The measurement principle, based on the differential permeation, and its procedure were described in a previous paper.[18] To resume, we presented classical behavior in Figure 2; the initially nil flux increased progressively with time up to a limit J_{st}, the stationary flux, which is typical of the steady state. This steady state was reached when the water contents that went in and went out of the membrane were equal, so that J_{st} was obtained from a plateau of the experimental flux curve. Usually the steady state corresponded to the maximum value of J (see Figure 2).

From the steady state (at the stationary flux J_{st}), it was possible to determine the permeability coefficient P

$$P = \frac{J_{st}L}{\Delta X} \tag{1}$$

where L was the thickness of the membrane and $\Delta X = \Delta a$ was the difference in activities between the two faces of the membrane. In our case, the upstream interface was in contact with liquid water (water activity $a_{up} = 1$) while the downstream interface was in contact with dry gas (water activity $a_{down} \approx 0$), so that $\Delta a \approx a_{up} = 1$. Usually P was expressed in Barrer (10^{-10} cm^3 STP·cm^{-1}·cm^{-2}·s^{-1}·cmHg^{-1}).

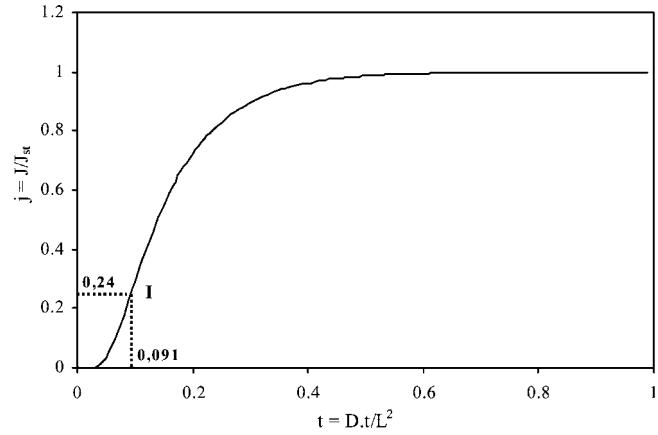

Figure 2. Theoretical curve of the flux with time integrating Fick's Law and assuming D constant.

The diffusivity could also be obtained from the permeation curve. This reduced curve $j = f(\tau)$ showed an inflection point I ($\tau_I = 0.091$, $j_I = 0.24$) (see Figure 2). At this inflection point I, the slope α ($= \Delta j/\Delta\tau$) depended on the D variation law. When D was constant, increased, or decreased with concentration, $\alpha = \alpha_0 = 5.82$, $\alpha > \alpha_0$ or $\alpha < \alpha_0$, respectively. The slope α could be used as a significant parameter of the concentration dependence. One of the main problems in transport phenomena was the determination of the ad-hoc value (or expression) of the diffusion coefficient D. If we assumed D as constant, its value could be calculated from the time $t_{0.24}$ corresponding to a value of $J/J_{st} = 0.24$, that is, at the inflection point I of the transient permeation curve (Figure 2) for which $\tau = 0.091$[19]

$$D_{0.24} = \frac{0.091L^2}{t_{0.24}} \tag{2}$$

When D was not constant, the diffusion coefficient was generally considered to increase exponentially with the local permeant concentration in the membrane during the course of water penetration and this variation of D was generally attributed to an increase of the free volume due to a plasticization effect of the materials by the permeant (water).[20,21]

b. CO_2 Time-Lag Permeation. The measurement of carbon dioxide permeation was based on the variable pressure method. During all experiments, the temperature was maintained at 25 °C. Before measurement, the permeation cell (XX45047 Millipore filtration cell adapted for gas permeation) was submitted to a vacuum (0.1 Pa) on both sides of the membrane at least for one day. Then, the upstream side was provided with the gas under test at pressure p_1 (in our case $p_1 = 4$ bar). The pressure increase (p_2) in the calibrated downstream volume was measured using a sensitive pressure gauge (0−1000 Pa, Effa AW-10-T4) connected to a data acquisition system. Pressure conditions were chosen in such a way that no irreversible structural modification by CO_2 plasticization effects[22] could appear in the tested membranes. When the upstream face of an initially dry membrane was suddenly into contact with an atmosphere at fixed carbon dioxyde pressure, while the downstream face was kept at a low pressure (under vacuum, 0.1 Pa), a carbon dioxide quantity Q occurred through the membrane.

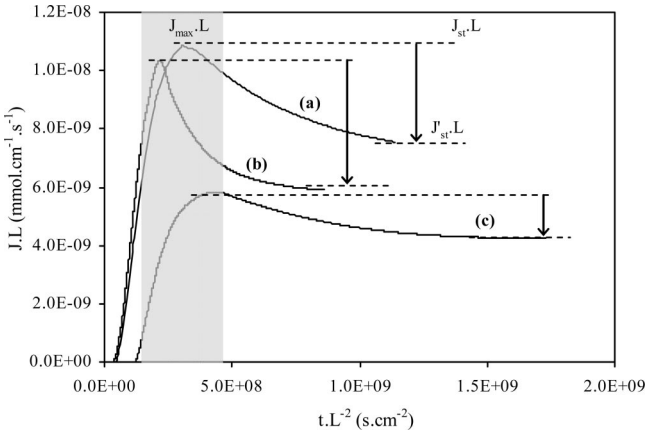

Figure 3. Thickness-corrected water flux (*JL*) permeating through polymer membranes as a function of the reduce time tL^{-2}: (a) the membrane with $L = 128$ μm, (b) the membrane with $L = 114$ μm, and (c) the membrane with $L = 76$ μm.

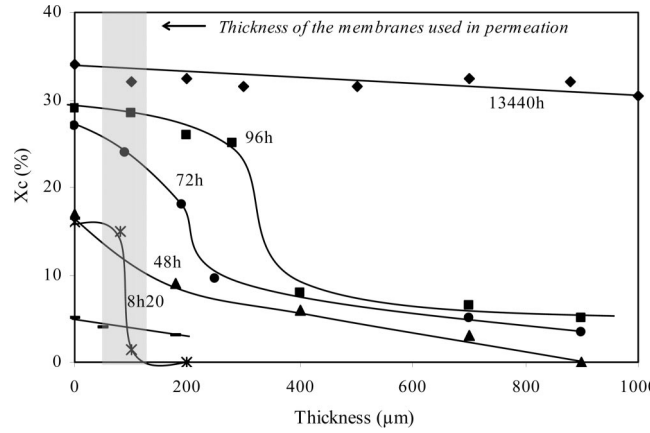

Figure 4. X_c (DSC determination) vs depth for plates immersed in water at various times. Dotted lines are guides for the eyes.

The initially nil concentration increased progressively with the time up to a steady state limit C_{eq}.

The permeability coefficient was determined from eq 1 with $\Delta X = \Delta p$, the pressure difference between the two faces of the membrane. P was calculated according to the following equation:

$$P = \frac{\mathrm{d}p}{\mathrm{d}t}\frac{LV}{ART\Delta p} \tag{3}$$

with V being the downstream volume, A is the exposed area, L is the thickness, R is the ideal gas constant, and $\Delta p \sim p_1 - p_2 \sim p_1$.[23]

As for water, one of the main problem in the determination of the values of the different quantities which occurred in these equations was linked to the determination of the ad-hoc value (or expression) of the diffusion coefficient D. However, in the case of gas and assuming no specific interaction between gas and polymer, such as carbon dioxide, the diffusion coefficient could be supposed constant. Usually, its value could be calculated from the time-lag t_L[24]

$$D_L = \frac{L^2}{6t_L} \tag{4}$$

For permeation measurements, uncertainties are mainly due to the thickness measurements errors, knowing that for water and gas permeation tests, the chilled mirror hydrometer and the pressure gauge are very sensitive (less than 0.5% of the measurement). From that the error in the permeability measurements are given in tables by taking into account the thickness errors.

Results and Discussion

1. Water Permeation. In the first step, we had studied by permeation tests three amorphous MXD6 membranes of different thickness. In Figure 3, we have plotted the thickness-corrected fluxes of water (*JL* where L is the membrane thickness) permeating through the polymer membranes as a function of the reduced time tL^{-2} when a water activity step (from zero to one) is applied on the upstream face of a membrane at time zero of the transient regime. This plot takes into account the effect of the membrane's thickness on the water diffusion and the permeation flux, so that the differences in the permeation patterns should represent the intrinsic behavior of the materials. The correction was based on the assumption that the materials were homogeneous, i.e. of uniform in properties; this assumption was acceptable insofar as the membranes were made of dense polymers and were not restricted to any specific orientation.

Two untypical phenomena can be observed at the maximum water flux ($J_{max}L$): (1) the stationary flux J_{st}, obtained at the steady state, is not reached at the maximum of J (as usually expected) and (2) the quantity, *JL*, depends on the thickness of the MXD6 membranes. Indeed, in our case, the quantity $J_{max}L$ varies with the membrane thickness (see Figure 3). Usually, the permeation kinetics of a homogeneous and dense polymer should not depend on the membrane thickness. In other words, the plot of a thickness corrected water flux *JL* should show the same stationary flux $J_{st}L$ (permeability coefficient) and the same kinetic variations. That was not the case with our samples.

In a previous work we had demonstrated by using the X-rays diffraction and DSC measurements that a spherulitic water-induced crystallization phase took place from the surfaces in the MXD6 plates after water immersion at ambient temperature. The degree of crystallinity was maximum at the polymer/water interface and decreased when the depth increased. At a given depth, the degree of crystallinity increases when the time of immersion increases (see Figure 4). With thickness membrane $L \approx 100$ μm close to those studied, we have shown that for an immersion duration lower than 8 h, the degree of crystallinity in mass X_c is negligible. However, for 8 h the degree of crystallinity at the surface becomes non-negligible (X_c is close to 16%). After 96 h, X_c is constant and is equal to 33%. The same tendency, an increase and then a decrease of water flux in comparable time scales, is observed for tested samples (Figure 3). This shows that the MXD6 membranes are characterized by the same intrinsic behavior to water molecules. We had to keep in mind that in permeation, the flux was measured just when the molecules had passed through the membranes thickness. As a consequence, from the water permeation curve it was not possible to correlate at time t the degree of crystallinity which appeared at the upper face with the water flux at downstream. The beginning of the crystallization started before the flux reached the classical plateau generally observed for many polymers. The reduced time tL^{-2} for time t equal to 8 h is indicated on the Figure 3 by the gray zone. This put in evidence that the water flux variations in this range of time are linked to the crystalline phase appearance. As it was well known

TABLE 1: Water Permeability for Three Amorphous MXD6 Membranes

thickness L (μm)	P (J_{max}) (barrer[a])	P' (J'_{st}) (barrer)
128	1038 ± 100	<720 ± 69
114	973 ± 105	<526 ± 57
76	549 ± 89	<398 ± 64

[a] 1 barrer = 10^{-10} cm^3 STP·cm^{-1}·cm^{-2}·s^{-1}·cmHg^{-1}.

that crystalline zones act as a barrier for molecule transport, the formation of the crystalline phase which occurred during the water permeation process led to reduce the mobility and the concentration of water molecules. In that way, the water flux slowed down going through a maximum quantity $J_{max}L$. Then, as crystals form, the permeation rate decreased that is, as long as the crystalline phase progresses in the material, the water flux, JL, decreased. The permanent regime $J'_{st}L$ (in Figure 3) was reached at longer time ($t > 40$ h). We could conclude that during the time needed for the progression of the crystalline phase in the membrane, J decreased and became constant when the membrane was completely crystallized.

The water permeability coefficient P was usually calculated from the stationary flux J_{st} (see eq 1), that is, at the steady state and for the higher value of J. However, as mentioned previously the situation was uncommon because of the permeation overshoot ($J'_{st} < J_{max}$) directly linked to the water-induced crystallization whose effect appeared for times closed to 8 h. From that, we had estimated a water permeability coefficient P' for longest duration, that is, at the stationary flux J'_{st}. The water permeability coefficients calculated for all permeation curves are gathered in Table 1. The analysis of these data shows that the barrier properties of MXD6 membranes are governed by the water-induced crystallization, which reduces significantly the water permeability.The fact that the water permeability depends on the membrane thickness can be easily explained by the crystalline phase profile (see Figure 4). For the same period of immersion in water and as long as the maximum is not reached, the degree of crystallinity X_c of the whole membrane is higher when its thickness is smaller. In that way, the water permeation through the thinner membrane induces a higher degree of crystallinity so that the maximum flux $J_{max}L$ is reached earlier. By taking into account the boundary conditions in the permeation process, the system was not in its equilibrium state. The gradient of water concentration inside the MXD6 membranes varied with the membrane thickness. Indeed, when the thickness of the membrane increased, the downside water concentration (in the dry state) in the last membrane layers was lower and so, because of the low effect of plasticization on the down face, the water-induced crystallization was reduced.

At the stage of the study, only one measurement of permeation had been performed for each amorphous membrane tested. Since the water-induced crystallization was an irreversible phenomenon, it became interesting to compare the water permeation behavior after a second permeation test for the same membrane. Before the second measurement, each sample was dried in an oven at 80 °C during 24 h. In Figure 5, we have plotted the thickness-corrected fluxes of water (JL) permeating through these polymer membranes as a function of the reduced time tL^{-2}; first measurement corresponding to the membrane initially amorphous and the second measurement to the same membrane but after undergoing the water-induced crystallization. For each tested membrane, the plot of a thickness corrected water flux JL obtained after the first and the second measurement does not exhibit the same behavior, that is, the same stationary flux $J_{st}L$ (permeability coefficient) and the same kinetic variations. In opposition to the first measurement, with the second passage the "typical" curve of permeation kinetic characteristic of a material independent of time (lack of a reduction in flux in the establishment of the steady state) is observed. The water flux curves obtained from the second permeation measurement show clearly the influence of crystals on the water barrier properties. Indeed, it can be observed that the drilling time (the time necessary for water molecules to reach the opposite side) for the second permeation test is higher than the first one and the quantity JL obtained at the steady state is lower for the water-induced crystallized membrane. The water permeability coefficients P calculated for all curves for each membrane are gathered in Table 2. The increase in the delay time of diffusion observed from the second passage and the significant reduction in water flux at the stationary state is explained by the initial conditions which differ between the first and second measurement. Indeed at the beginning of the second measurement, the material is already crystallized so that the concentration profile of water is reduced compared to the first experiment. The barrier effect should result in the increase of tortuosity (diffusion path). Indeed during the first measurement the crystallization occurred from only one face which was in contact with liquid water. Thus the gradient of water concentration between both sides of the membrane led to a non-symmetrical crystallization inside the membrane. Moreover it was interesting to note that for our studied samples the stationary flux reached during the second measurement, that is, when the material was highly crystallized by water (X_c close to 30%), was not the same for the three tested samples (Figure 5) and that confirmed the permeability of the material depended on the membrane thickness and its history occurred during the permeation process.

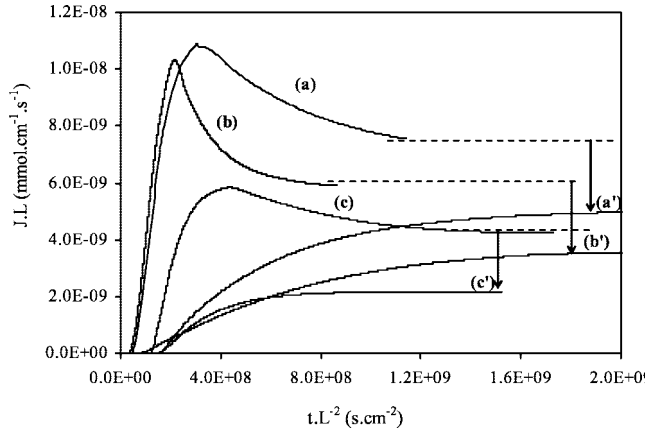

Figure 5. Thickness-corrected water flux (JL) permeating through three polymer membranes as a function of the reduce time tL^{-2}: (a) and (a′) first and second measurement for the membrane with $L = 128$ μm, (b) and (b′) first and second measurement for the membrane with $L = 114$ μm, and (c) and (c′) first and second measurement for the membrane with $L = 76$ μm.

From a kinetic point of view, it was easy to show the diffusion coefficient variation (with time or with the penetrant concentration in the polymer) when transient permeation data were available; the diffusion coefficient values calculated at different extents of the transient permeation of constant diffusion coefficient were no longer the same.[25] Since our binary system (water/MXD6) evolved due to the water-induced crystallization, it was clear that the diffusion process was dependent on time and consequently was non-Fickian diffusion. However some assumptions remained valid; the polymer was dense (material without porosity at the microscopic scale), the mass transfer occurred mainly in the perpendicular direction to the plane sheet

TABLE 2: Water Permeability and Diffusivity for MXD6 Membranes before and after Water-Induced Crystallization, and for a MXD6 Membrane Thermally Crystallized at 180°C during 3 h

thickness L (μm)			P (J'_{st}) (barrer)	$D_{0.24} \times 10^{10}$ ($cm^2 \cdot s^{-1}$)
128	membranes initially amorphous	first measurement	720 ± 70	11.1
		second measurement	464 ± 45	3.2
114		first measurement	526 ± 57	13.5
		second measurement	338 ± 36	3.3
76		first measurement	398 ± 64	5.7
		second measurement	155 ± 25	2.4
104	thermally crystallized		44 ± 5	1.5

(thin thickness), and the sorption of the penetrant at the membrane interface was much faster than the diffusion in the material, which was the rate determining step, so the interfacial sorption equilibrium was instantaneous and steady. Moreover, the swelling effect with time was not so high. During the water permeation process, when the membrane was in contact with liquid water (water activity $a = 1$), the increase of the membrane thickness never exceed 2%. From a recent study,[10] we could assume that for short times (<4 h) the diffusion seemed not to be affected by water-induced crystallization, since the degree of crystallinity was negligible and a time delay existed between incoming and outcoming fluxes. With our water/MXD6 system, the diffusion coefficient D was not constant and it was rather difficult to calculate the mean integral diffusion coefficient $<D>$ since the material evolved with water concentration and with time. The solubility and diffusivity were different in the crystalline and in the amorphous regions. It was usually expressed $D = D_a(1 - X_c)$ and $S = S_a(1 - X_c)$ where D_a and S_a were the solubility and diffusivity coefficients of the amorphous region.[26] In general, it was admitted that crystalline regions were barrier toward molecules such as water molecules. Thus, assuming that the penetrant was excluded from the crystals, the fact that a flux of water existed through the MXD6 membrane and this after water-induced crystallization meant that some amorphous regions remained open to water molecules but with an increase of tortuosity due to the presence of the crystalline zones. In terms of water permeation, taking into account the dependence of D with concentration and with time, the water/MXD6 system could not be simulated on the basis of Fick's Laws and was, for the moment, too complex to be simulated. At this stage of the work, we had not enough information (such as the velocity of the moving boundary) to simulate water flux curves in overall. A mathematical model for diffusion with induced crystallization had been developed for sorption measurements (but not in permeation) in the case of highly swollen polymers such as PET plasticized by organic solvents[27] which was not the case in our system polymer/penetrant (water had a lower plasticization effect). However, in the first period of permeation, that is, at the beginning of the transient permeation, the diffusion was not yet affected by the water-induced crystallization with starts later (8 h). From that, it was interesting to show the deviation between our experimental results (beginning flux curves) and the Fickian behavior with D constant (Figure 6). In that way, to compare experimental and theoretical results, the dimensionless time scale $\tau_{0.24}$ was used and defined as

$$\tau_{0.24} = \frac{D_{0.24}t}{L^2} \tag{5}$$

with $D_{0.24}$ being the water diffusion coefficient for which $J/J_{max} = 0.24$ and calculated according to eq 2. This $D_{0.24}$ value calculated on the Fickian basis with D constant corresponded to the beginning of the transient regime, keeping in mind that in this short time scale the water flux was not really affected by the few formed crystals. This comparison allowed one to show the change in the diffusion with the permeation extent. The calculated values $D_{0.24}$ are given in Table 2. As shown in Figure 6, for time higher than $\tau_{0.24}$ an important deviation is observed between experimental and calculated Fickian curves. This deviation reveals an increase in the water diffusivity with concentration. Such increase is generally attributed to a plasticization phenomenon leading to an increase of the free volume.[15] In our case, the plasticization of the MXD6 membrane by water allows a decrease of T_g which permits at ambient temperature, the crystallization to occur. From Figure 6, for the second measurement it is interesting to observe a deviation between experimental curve and the calculated flux with D constant. In this case for time higher than $\tau_{0.24}$, the experimental flux is found lower than the theoretical flux. In other words, for the second measurement, that is, when the membrane is already water-induced crystallized, the plasticizing effect is significantly reduced. Indeed, the amorphous phase degree is higher with the first permeation test than with the second one. The decrease of the $D_{0.24}$ values after the second water permeation measurement points out an increase of the tortuosity due to the presence of the crystalline zones (Table 2).

From the idea that the water permeability depended on the membrane thickness characterized by a gradient of water concentration and resulting from a degree of crystallinity which varied with the thickness, it was interesting to measure the water permeation flux from the other side of the membrane. For that, the same membrane had been tested in water permeation five times; four consecutive passages of water in one side and the fifth passage were done in the other side of the MXD6 membrane (see Figure 7). The first and second passage of water was already discussed previously (Figure 5). Since the third and

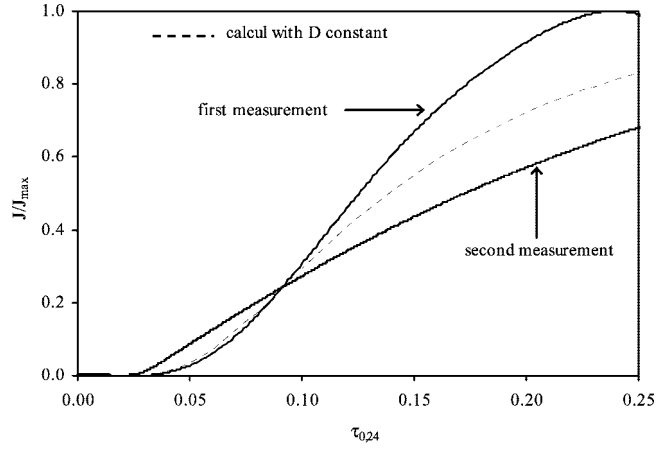

Figure 6. Water flux curves, plotted in the reduced scale J/J_{st} as a function of a dimensionless time $\tau = \tau_{0.24} = D_{0.24}t/L^2$ for $L = 114$ μm.

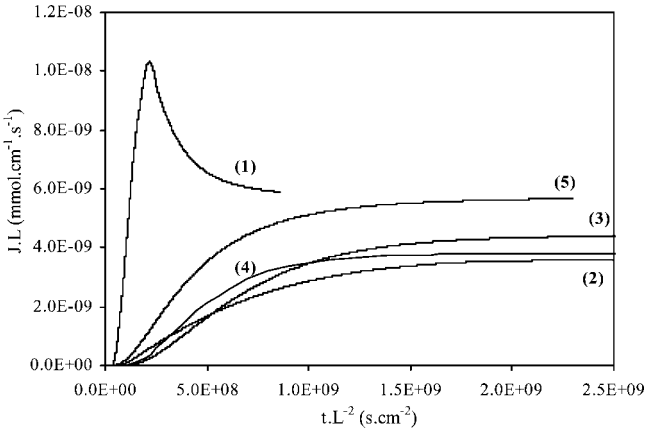

Figure 7. Thickness-corrected water flux (*JL*) permeating through a MXD6 membrane ($L = 114$ μm) for five passages of water as a function of the reduce time tL^{-2}: (1) passage 1, (2) passage 2, (3) passage 3, (4) passage 4, and (5) passage 5 returned.

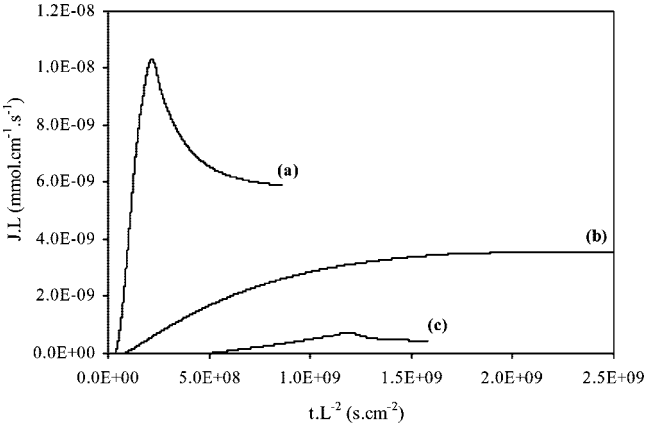

Figure 8. Thickness-corrected water flux (*JL*) permeating for (a) the MXD6 amorphous membrane ($L = 114$ μm), (b) the second passage of water of MXD6 membrane ($L = 114$ μm), and (c) the MDX6 membrane thermally crystallized at 180 °C during 3 h as a function of the reduce time tL^{-2}.

the fourth passages of water were obtained with the same face of the membrane in contact with liquid water, it was not surprising to observe practically the same typical water flux permeation. On the other hand, for the fifth passage, when the water permeation was measured on the other side of the membrane, we observed a slight increase of the flux and a decrease of the delay time of diffusion (Figure 7). This behavior was very consistent with the presence of a gradient of crystallinity in the thickness of the sample. Indeed, the water-induced crystallization that occurred during the permeation process led to a degree of crystallinity that decreased from one side (face in contact with liquid water) to the other side (face in contact with nitrogen). From that, for the fifth passage the face of the membrane in contact with liquid water was characterized by a reduced crystallinity degree (in comparison with the other side) and thus the water concentration inside the first layers of the membrane became higher than that of the other side of the membrane allowing a higher flux of water. Concerning the barrier effect, it was then interesting to compare the water permeability of water-induced crystallized MXD6 with another thermally crystallized MXD6. The experimental water permeation curves obtained from amorphous, water-induced and thermally crystallized sample are given in Figure 8. As we can observe, the MXD6 membrane is less permeable when thermally crystallized than crystallized by water. Although the membrane

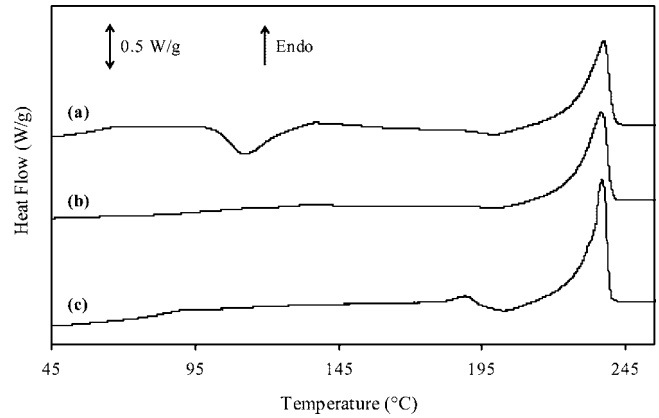

Figure 9. DSC heating curves (10 K min^{-1}) for (a) the MXD6 amorphous membrane before the first passage, (b) the MXD6 membrane after the second passage of water, and (c) the MXD6 membrane thermally crystallized at 180 °C during 3 h.

is already thermally crystallized, the shape of the permeation kinetic seems to reveal the water-induced crystallization that is highlighted by a slight decrease of the flux after reaching a maximum. This result would indicate that in spite of the presence of crystallites in the membrane, the MXD6 is able to plasticize with water and so forms new crystals during the water permeation process whereas with a membrane initially crystallized by water, during the second passage a typical water flux is observed without new water-induced crystallization. To explain such difference, we had to consider that the crystals due to the water-induced crystallization were not scattered homogeneously in the thickness of the membrane, which is opposite with the crystals formed during the thermal process. In this case, the thermally crystallized material that was already not very permeable became more barrier (see Table 2). We could attribute the difference between the two permeation curves to two causes: (a) because of the higher presence of crystals in front of the thickness of the membrane crystallized by water compared to thermally crystallized one, the water concentration profile was so reduced in the first layers of the membrane that the water molecule contents was not sufficient to plasticize the material; (b) secondary crystals existed in the thermal crystallized sample and probably increased the tortuosity of the material.

In Figure 9 are reported the DSC curves of amorphous, water-induced and thermally crystallized samples. For the amorphous material, following four thermal events can be observed: the glass transition appears for 78 °C < T_g < 93 °C evidenced by the endothermic heat capacity jump ΔCp, the thermal cold crystallization is revealed by an exothermic phenomenon lying between 95 and 140 °C, then a second weak exothermic phenomenon appears around $T = 205$ °C. Finally, the melting of the crystalline phase revealed by an endothermic peak occurs between 205 and 244 °C. For the polymers that presented the same DSC data variations, the exothermic peak just below the endotherm was generally attributed to a polymorphism[15] or to a crystalline reorganization.[16] From a previous study using DSC and X-ray analysis,[10] this exothermic peak had to be attributed to crystalline reorganization. Indeed, when the sample was crystallized from the glassy state as during a DSC scan, the formed crystals were imperfect and therefore relatively prone to be reorganized during heating to a crystal population with a higher thermodynamic stability. The exothermic peak of crystallization does not appear for curve (b) and (c) because the samples are crystallized prior to analyze. For the water-induced crystallized sample, the glass transition and the exothermic peak

TABLE 3: Carbon Dioxide Permeability for MXD6 Membranes before and after Water-Induced Crystallization and for a MXD6 Membrane Thermally Crystallized at 180°C during 3 h

MXD6	permeability × 10^3 (barrer)	crystallinity X_c (%)
amorphous	1.1 ± 0.1	7.5
crystallized by water	0.7 ± 0.08	20
thermally crystallized	0.3 ± 0.04	22

due to crystalline reorganization are very weak. The peak of fusion looks similar of the peak of sample (a). For MXD6 samples thermally crystallized, the glass transition is less observable and appears at higher temperature while a new endothermic peak appears. This endothermic peak at 190 °C can be attributed to the melting of secondary lamellae and appears generally just above the crystallization temperature (here 180 °C). The peak of fusion is different of the peak of fusion of curve (a). It is due to the difference of thermal history.[10] From enthalpies associated with endothermic and exothermic peak, the degrees of crystallinity were calculated ($X_c = 22$ and 20% for thermally induced and water-induced crystallized MXD6, respectively, Table 3). As the degrees of crystallinity were very close, we could investigate the effect of the crystallization process (which had induced different microstructure) and not the effect of the percentage of crystalline phase. Indeed, it was well known than the crystalline microstructure was dependent on various parameters and in particular the temperature at which the crystallization process occurred. It had been shown on various semicrystalline polymers, such as MXD6, PP,[28,29] PET,[30] PLLA[31], that for crystallization from the melt or from the glassy state (i) the size of the spherulites increased with T_c, and (ii) the size of the crystalline lamellae increased with T_c. So, we could suppose than crystalline lamella were more perfect for the thermally crystallized samples (crystallized at T_c = 180 °C) with presence of secondary crystallites than for the water-induced crystallized one (T_c = 25 °C).

2. CO_2 permeation. In terms of application, the water-induced crystallization and the thermally crystallization should improve the gas barrier properties of the material. From that it was interesting to examine the carbon dioxide permeation through MXD6 membranes and compare their behavior for the different states: amorphous, crystallized by water (during one week at 25 °C), and thermally crystallized (during 3 h at 180 °C). The carbon dioxide permeation results are plotted in Figure 10 and gathered in Table 3. As expected, the gas barrier properties of MXD6 membranes are confirmed from the very low values of P with the crystallized membranes being less permeable to CO_2 than the amorphous one. By comparing both crystallized materials, we could note that in terms of gas barrier properties, the thermal crystalline phase was more efficient than the water-induced crystalline one. This result was consistent with the water permeation properties. In other words, the barrier properties of semi-crystalline MXD6 membranes depended on their crystalline microstructures. According to the crystallization process (thermal and induced by water), the size and the morphology of the crystalline phase could change. In our case, for practically the same degree of crystallinity the fact that crystalline lamella might be more perfect for the thermally crystallized samples with presence of secondary crystallites than for the water-induced crystallized ones could easily explain the improvement of the barrier properties of the material.

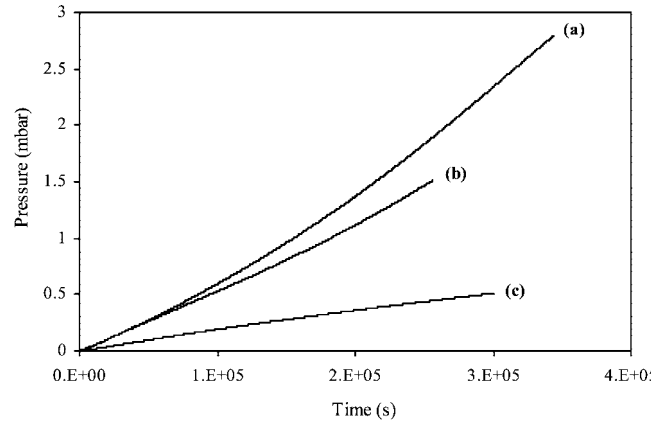

Figure 10. Carbon dioxide permeation through different MXD6 membranes: (a) an amorphous membrane before the crystallization by water, (b) the same membrane crystallized by water (during one week at 25 °C) and dried at 80 °C, and (c) a membrane crystallized at 180 °C during 3 h.

Conclusion

The chemical interactions between water molecules and molecular hydrogen bonding led to strongly reduce the inter-chain interactions increasing the free volume and consequently increased the diffusivity (well-known plasticization effects). For MXD6 membranes, an additional effect took place. When the water molecules had sufficiently penetrated into the polymer, a spherulitic crystallization could appear at room temperature (i.e., 60 °C below the glass transition temperature of the dry material). So, the permeation test of an initially amorphous membrane could be very unusual in presence of water. After reaching a maximum, the permeability to water decreased as long as the crystalline phase progressed in the membrane depth until reaching a permanent regime. The water flux curves obtained for the same membrane tested two times showed a specific behavior highlighting the water-induced crystallization during the first analysis. The quasi-linear dependence of the water permeability P (J_{max}) with the samples thickness was linked to the fact that the crystallization took places from the interface water/polymer and not in the bulk sample. The presence of crystals improved the water barrier properties of MXD6 membranes. Indeed, the water permeability went from 398 barrer for an amorphous MXD6 to 155 barrer for a semicrystalline one. Because of the water-induced crystallization and water plasticization opposite effect, the diffusivity D was not a constant. The presence of the crystalline phase (which reduced the diffusivity) limited the increase of D resulting from the plasticization effect which occurred in the amorphous regions.

In this work, we had shown that the presence of a crystalline phase could have different effect on the barrier properties. We had studied semicrystalline MXD6 with two different crystalline microstructures: the first crystalline phase had appeared in a plasticized amorphous matrix at room temperature and the second had appeared from the melted at high temperature. We had shown that the difference of microstructure (presence of secondary crystallites for thermally induced crystalline phase) had an important influence on water and CO_2 barrier properties. The secondary crystallites probably increased the tortuosity for permeant molecules.

References and Notes

(1) Boutroy, N.; Pernel, Y.; Rius, J. M.; Auger, F.; Von Bardeleben, H. J.; Cantin, J. L.; Abel, F.; Zeinert, A.; Casiraghi, C.; Ferrari, A. C.; Robertson, J. *Diamond Relat. Mater.* **2006**, *15*, 921–927.

(2) Bieder, A.; Gruniger, A.; Von Rohr, R. *Surf. Coat. Technol.* **2005**, *200*, 928–931.

(3) Erlat, A. G.; Henry, B. M.; Grovenor, C. R. M.; Briggs, A. G. D. *J. Phys. Chem. B* **2004**, *108* (3), 883–890.

(4) Chung, J. W.; Son, S-B.; Chun, S-W.; Kang, T. J.; Kwak, S-Y. *Polym. Degrad. Stab.* **2008**, *93*, 252–259.

(5) Fermeglia, M.; Cosoli, P.; Ferrone, M.; Piccarolo, S.; Mensitieri, G.; Pricl, S. *Polymer* **2006**, *47*, 5979–5989.

(6) Uddin, A. J.; Ohkoshi, Y.; Gotoh, Y.; Nagura, M.; Endo, R. *J. Polym. Sci., Part B: Polym. Phys.* **2004**, *42*, 433–444.

(7) Miyamoto, A. *Polymer Data Handbook*; Oxford University Press: New York, 1999; p 230.

(8) Ben Doudou, B.; Dargent, E.; Grenet, J. *J. Plast. Film Sheeting* **2005**, *21*, 233–251.

(9) Dargent, E.; Denis, A.; Galland, C.; Grenet, J. *J. Therm. Anal.* **1996**, *46*, 377–385.

(10) Ben Doudou, B.; Dargent, E.; Grenet, J. *J. Therm. Anal. Calorim.* **2006**, *85*, 409–415.

(11) Kawasaki, K.; Sekita, Y. *J. Polym. Sci., Part A: Polym. Chem.* **1964**, *2*, 2437–2443.

(12) Saiter, J. M.; Langevin, D.; Lebaudy, P.; Grenet, J. *J. Non-Cryst. Solids* **1994**, *172/174* (1), 640–643.

(13) Langevin, D.; Grenet, J.; Saiter, J. M. *Eur. Polym. J.* **1994**, *30*, 349–355.

(14) Adriaensens, P.; Pollaris, A.; Carleer, R.; Vanderzande, D.; Gelan, J.; Litvinov, V. M.; Tijssen, J. *Polymer* **2001**, *42*, 7943–7952.

(15) Ben Doudou, B.; Dargent, E.; Marais, S.; Grenet, J.; Hirata, Y. *J. Polym. Sci., Part B: Polym. Phys.* **2005**, *43*, 2604–2616.

(16) Lagaron, J. M.; Gimenez, E.; Gavara, R.; Saura, J. J. *Polymer* **2001**, *42*, 9531–9540.

(17) Dreux, F.; Marais, S.; Poncin-Epaillard, F.; Métayer, M.; Labbé, M. *Langmuir* **2002**, *18*, 10411–10420.

(18) Métayer, M.; Labbé, M.; Marais, S.; Langevin, D.; Brainville, M.; Chappey, C.; Dreux, F.; Belliard, P. *Polym. Test.* **1999**, *18*, 533–549.

(19) Marais, S.; Métayer, M.; Labbé, M. *J. Appl. Polym. Sci.* **1999**, *74*, 3380–3395.

(20) Prager, S.; Long, F. A. *J. Am. Chem. Soc.* **1951**, *73*, 4072–4075.

(21) Stern, S. A.; Trohalaki. S. *In Barrier Polymers and Barrier Structures*; Korros, W. J., Eds.; ACS Symposium Series 423; American Chemical Society: Washington DC. 1990; pp 22−59.

(22) Wessling, M. Ph.D Thesis, University of Enschede, The Netherlands, 1993.

(23) Marais, S.; Saiter, J. M.; Devallencourt, C.; Nguyen, Q. T.; Métayer, M. *Polym. Test.* **2002**, *21*, 425–431.

(24) Frisch, H. L. *J. Polym. Sci.* **1957**, *61*, 93–95.

(25) Watson, J. M.; Payne, P. A. *J. Membr. Sci.* **1990**, *49*, 171–185.

(26) Van Krevelen, D. W. In *Properties of Polymers*, 3rd ed.; Elsevier Science: New York, 1997; pp 1−861.

(27) Durning, C. J.; Russel, W. B. *Polymer* **1985**, *26*, 131–140.

(28) Chen, Y.; Chen, Y.; Yang, D. *Polymer* **2006**, *47*, 1667–1673.

(29) Álvarez, C.; Martínez-Gómez, A.; Pérez, E.; de la Orden, M. U.; Martínez Urreaga, J. *Polymer* **2007**, *48*, 3137–3147.

(30) Flores, A; Pieruccini, M.; Stribeck, N.; Funari, S. S.; Bosch, E.; Balta-Calleja, F.-J. *Polymer* **2005**, *46*, 9404–9410.

(31) Wang, Y.; Funari, S. S.; Mano, J. F. *Macromol. Chem. Phys.* **2006**, *207*, 1262–1271.

JP810241Z